

Temperature and density dependence of the linewidths and line shifts of the rotational Raman lines in N₂ and H₂

G. C. Herring, Mark J. Dyer, and William K. Bischel

Chemical Physics Laboratory, SRI International, Menlo Park, California 94025

(Received 10 February 1986)

The temperature and density dependence of the rotational Raman linewidths and line shifts for the diatomic molecules N₂ and H₂ has been measured using stimulated Raman gain spectroscopy. Room-temperature results for the density-broadening coefficients, B , in N₂ are compared with *ab initio* calculations, while the low-temperature (80 and 195 K) results are the first to be reported, to our knowledge. Values of γ in the relation, $B \propto T^\gamma$, were determined from fits to the data for self-broadening in N₂ yielding $0.25 < \gamma < 0.39$. Foreign-gas (O₂) broadening coefficients for the N₂ transitions were also measured and found to be 10–15% smaller than the self-broadening coefficients. Our linewidth and line-shift results for H₂ are in general agreement with previous measurements.

I. INTRODUCTION

Modeling the rotational Raman gain in N₂ is of interest since stimulated Raman scattering will alter the mode quality of a high-intensity beam propagating through air.¹ Accurate knowledge of the Raman linewidths is necessary² for any useful model because the steady-state Raman gain is inversely proportional to the linewidth. Results of previous studies^{3–7} of the room-temperature rotational Raman linewidths in N₂ typically differ by 30%, while results at other temperatures have not been reported. The main purpose of this work is to measure the temperature dependence of the linewidths and line shifts for the rotational Raman transitions (*S* branch) in N₂.

This work differs from previous measurements of rotational Raman linewidths^{3–7} in three aspects. First, we have measured the temperature dependence of the line broadening over the range 80–300 K. Previous work in N₂ has been only for room temperature. Second, the densities, used in this work (0.01–2.0 amagat) are 2 orders of magnitude lower than those (1.0–100 amagat) used in previous measurements. Complications due to overlapping of adjacent lines are eliminated by working at lower densities where the Raman lines are typically separated by 100 linewidths. Finally, all previous measurements have used spontaneous Raman scattering, whereas we have used stimulated Raman scattering, which has a frequency resolution several orders of magnitude higher than its spontaneous counterpart.

This paper reports experimental results for line-broadening and line-shift coefficients for Stokes rotational Raman transitions in N₂ and H₂. Results are presented for the even-*J* transitions, *S*(2) through *S*(16), at temperatures of 80, 195, and 295 K in N₂ and for *S*(0) and *S*(1) at temperatures of 80 and 295 K in H₂. The foreign-gas (O₂) broadening and shifts of the four strongest N₂ transitions have also been measured at 195 and 295 K. The room-temperature broadening coefficients in N₂ are compared with *ab initio* calculations, whereas the low-temperature N₂ self-broadening and the O₂ foreign-gas results are the first to be reported to our knowledge. The present tem-

perature dependence of N₂ is compared to that found in studies of CO and CO₂. Finally the present H₂ results are compared with previous measurements.

II. EXPERIMENTAL PROCEDURE

A. Apparatus

An overview of the experimental setup is shown in Fig. 1. This quasi-cw stimulated Raman spectrometer is similar to that developed by Esherick and Owyong⁸ and consists of a cw probe laser, a tunable, pulsed pump laser, a pair of gas (sample and reference) cells, and fast photodiodes to detect the induced Raman gain on the probe beams.

The probe laser is a Kr⁺-ion laser, operating at 568 nm and forced into single-mode operation with the insertion of a temperature-stabilized etalon into the cavity. This laser has a time-averaged linewidth less than 30 MHz. The probe beam was split into two equal intensity beams so that Raman signals could be simultaneously obtained from two separate gas samples. After passing through their respective sample cells, both of the cw probe beams were chopped at 10 Hz with a mechanical chopper (not shown in Fig. 1). This resulted in 170- μ sec square-wave pulses that were incident on the photodiodes. Chopping of the probe increases the saturation intensity for the photodiodes. The average power of the probe beams was 150 mW in both the sample and reference cells.

The pump laser was a tunable, single-mode (1-MHz linewidth) cw dye laser that was pulse amplified using a Quanta-Ray PDA-1. The cw dye laser input to the PDA-1 was typically 400 mW. The PDA-1 was pumped with the 532-nm output (130 mJ per pulse) from a frequency-doubled YAG laser (where YAG denotes yttrium aluminum garnet). At 565 nm, the tunable output of the PDA-1 consisted of 2-mJ, 10-nsec [full width at half maximum (FWHM)] pulses at 10 Hz. The linewidth of the pump laser was 100 MHz, about a factor of 2 larger than the Fourier transform for a 10-nsec pulse. Peak pump intensities at the focal planes were estimated to be 5

GW/cm² in the sample cell and 70% of that in the reference cell.

The pump probe beams were mode-matched and then were focused and crossed in the gas cells using 40-cm focal length lenses. The crossing angle was 1.0° in both of the cells. A series of diaphragms placed around the probe beams was used to eliminate scattered pump light. Both probe beams were monitored with reverse-biased photodiodes that had rise times of less than 1.0 nsec, and were terminated with 50-Ω resistors. The total probe power incident on the photodiodes during the 170-μsec probe-laser pulses was 10 mW. Capacitors (300 pF) were used to block the 170-μsec pulses and to pass the 10-nsec Raman signals. These signals were amplified by a factor of 100 and then averaged with gated integrators. Output time constants for the integrators and total scan times were usually 0.5 sec and 4 min, respectively. Occasionally, for weak transitions, time constants and scan times were increased to 2.5 sec and 10 min, respectively. After the pump beam exited the reference cell, it was also monitored with a third photodiode. This signal was used to normalize the two Raman signals for slow-pump power variations during the scans.

The sample cell was constructed by attaching a pair of 3.0-cm-diam Brewster window extensions to a drilled-out 10 cm³ cube of aluminum. One face of the aluminum cube is in contact with a second reservoir that can be filled with either liquid N₂ or an acetone dry-ice bath. The cooled sample cell was insulated with a vacuum, and the temperature was monitored with a thermocouple that was imbedded in the aluminum cube. The reference gas cell was kept at room temperature and a pressure of 10 Torr for N₂ scans and 200 Torr for most of the H₂ scans.

The temperature dependence of the linewidths and line shifts was measured by taking measurements at three temperatures: 80, 195, and 295 K. At each temperature the line shape was recorded for several densities over the range 0.01–2.0 amagat. For the low-temperature runs, there was a time period ranging from a few to 15 minutes between scans with different densities, so that any gas added between scans always had sufficient time to come to thermal equilibrium with the cell. For each set of runs at constant temperature, the density was randomly changed rather than constantly adding or eliminating gas from the sample cell for each succeeding run.

The pressure in the experimental cells was measured using a 10 000-Torr MKS Baratron gauge, and the temperature was measured using a Chromel-Alumel thermocouple referenced to 273 K. The density for both N₂ and H₂ was calculated using the perfect gas law since the density calculated using the second virial coefficient⁹ deviates from this calculation by less than 1% at the densities and temperatures used in these experiments.

B. Data analysis

All of the experimental line shapes were fit to either Voigt or Lorentzian profiles rather than the more accurate Galatry profile,¹⁰ which accounts for Dicke narrowing. Using the Voigt profile is a good approximation for the N₂ rotational transitions studied here since the

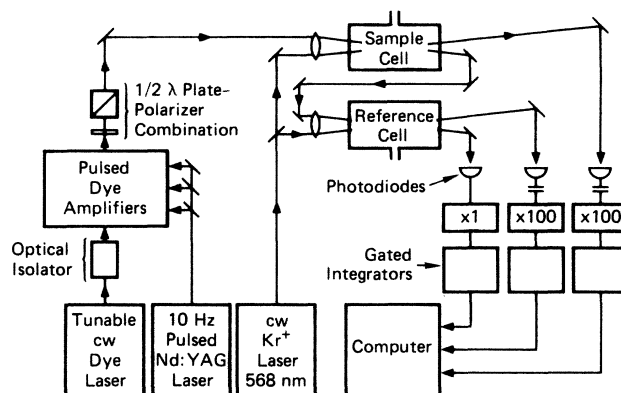


FIG. 1. Schematic of experimental apparatus for quasi-cw stimulated Raman spectroscopy.

Doppler broadening (5 MHz), and hence the Dicke narrowing, is negligible. This is also a good approximation for the H₂ transitions, since the instrumental width typically accounts for one-half the total linewidth and uncertainties in the instrumental linewidth will mask the small difference between the Voigt and Galatry profiles. Thus we have used Voigt profiles to fit our data using the procedure described here.

Since the laser linewidth was comparable to the low-density Raman linewidth, it was important to account for this instrumental width in the data analysis. Although the pump-laser frequency profile was not directly measured, it was indirectly determined by scanning the laser over a narrow Raman line [e.g., S(0) in H₂ at 5 Torr]. This transition has negligible (1 MHz) collisional broadening compared to 100 MHz of Doppler broadening. The profile for this transition was found to fit extremely well to a pure Gaussian. Since the convolution of two Gaussians results in another Gaussian, we concluded that the pump-laser profile could be approximated as a Gaussian. Fitting Voigt profiles to low-density, narrow N₂ line profiles with known Doppler and Lorentzian contributions confirmed this conclusion. The probe-laser linewidth was assumed to be negligible when convolved with the pump linewidth; thus all the data presented here were analyzed

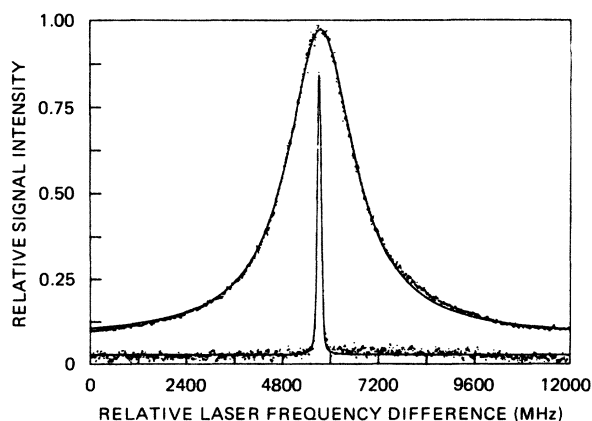


FIG. 2. Example of S(10) line shape in N₂ at 295 K and 10 Torr (narrower profile) and at 195 K and 400 Torr (wider profile). Individual dots are data and the solid lines are Voigt fits.

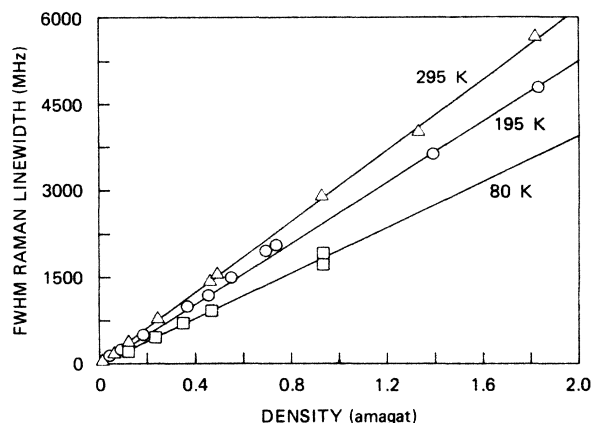


FIG. 3. $S(10)$ linewidths in N_2 at temperatures of 80 K (\square), 195 K (\circ), and 295 K (\triangle). Solid lines are linear least-squares fits to the data.

assuming a Gaussian profile for the instrumental width.

The fitting procedure used to determine the Lorentzian portion of the line shapes was different for the N_2 and H_2 data. We first describe the fitting procedure for the N_2 transition. For high densities in N_2 , Doppler broadening (5 MHz) and the laser linewidth (100 MHz) can be neglected. This fact is confirmed with the following result: Fitting Voigt profiles with freely varying Lorentzian and Gaussian parameters to our higher density (greater than 0.1 amagat) data gave negligible Gaussian components. Thus sample cell line shapes for high densities were first fitted to pure Lorentzians to get a first approximation to the Lorentzian width. The low-density reference cell data were then fitted to Voigt line shapes with a fixed Lorentzian (determined from the high-density fits) and variable Gaussian components. This Gaussian component, representing the pump-laser profile for that particular scan, was then used in a final Voigt fit to the sample cell profile. Any fluctuations in the pump-laser linewidth from scan to scan were accounted for with this procedure. These Gaussian components were typically within ± 20 MHz of an approximate average value of 100 MHz. The change in Lorentzian linewidth determined from the first Lorentzian fit and the final Voigt fit was

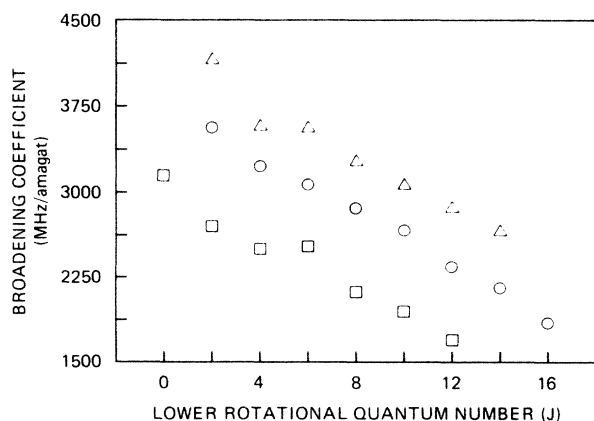


FIG. 4. J dependence of the N_2 rotational Raman broadening coefficients for 80 K (\square), 195 K (\circ), and 295 K (\triangle).

TABLE I. Temperature dependence of the self-broadening coefficients for the rotational Raman lines of N_2 .

$S(J)$	B (MHz/amagat)		
	295 K	195 K	80 K
0		4730 \pm 700	3140 \pm 470
2	4160 \pm 400	3560 \pm 350	2700 \pm 270
4	3580 \pm 60	3230 \pm 320	2490 \pm 250
6	3560 \pm 30	3070 \pm 30	2520 \pm 40
8	3270 \pm 60	2860 \pm 30	2120 \pm 60
10	3060 \pm 60	2660 \pm 30	1940 \pm 40
12	2870 \pm 50	2340 \pm 260	1690 \pm 100
14	2660 \pm 270	2150 \pm 215	
16		1840 \pm 185	

typically a few percent and further iterations were not necessary.

For the H_2 transitions studied, experimental constraints did not allow the density in the cell to be larger than 3 amagat. Therefore the approximate density-broadening coefficient could not be determined from the high-density data. Hence, the above procedure was not applicable. Instead, all of the H_2 line shapes were fitted to Voigt profiles with freely adjustable Lorentzian and Gaussian components.

III. RESULTS

A. Line broadening in N_2

An example of the $S(10)$ Raman profile in N_2 is shown in Fig. 2. The narrower profile was taken at 10 Torr and 295 K and the wider profile was taken at 400 Torr and 195 K. Individual dots represent the data, and the solid line represents the fit for a Voigt line shape, which is dominated by its Lorentzian component for the 400-Torr data. A slight asymmetry is observable in the data of Fig. 2 and was characteristic of most of the N_2 data obtained. An asymmetry of this magnitude will not have an appreciable effect on the linewidth determinations, but could produce significant systematic errors in the line-shift determinations because the line shifts are so small. This asymmetry is discussed later in Sec. III C.

For densities larger than 0.004 amagat (~ 3 Torr at 298 K), the rotational Raman lines of N_2 are collision broadened giving a Lorentzian line-shape function. Hence, the linewidth will be a linear function of density. We have therefore taken the Lorentzian component resulting from the data-fitting procedure described in Sec. II B

TABLE II. Comparison of different measurements of the room-temperature self-broadening in N_2 .

$S(J)$	B (MHz/amagat)			
	Present work	Ref. 3	Ref. 6	Ref. 7
2	4160 \pm 400	3370		
4	3580 \pm 60	3050	2590	3280 \pm 300
6	3570 \pm 30	3050		
8	3270 \pm 60	2660	2300	3150 \pm 300
10	3070 \pm 60	2590		
12	2870 \pm 50	2400	1980	2820 \pm 300
14	2660 \pm 270	2205		
16		2080		

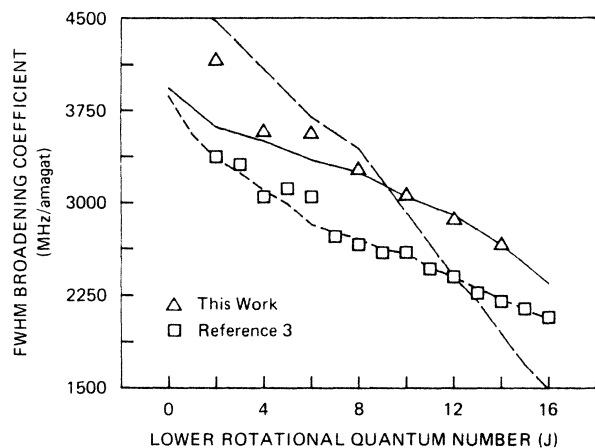


FIG. 5. Comparison of theoretical calculations with experimental data for collisional broadening of the rotational Raman lines in N_2 at room temperature. The calculations are from Ref. 11 (long dash), Ref. 12 (short dash), and Ref. 13 (solid line). The experimental data are from Ref. 3 (\square) and this work (\triangle).

and determined the density-broadening coefficients B for each temperature studied by fitting the linewidths to a straight line. The data and the linear fit (solid line) for the $S(10)$ transition are given in Fig. 3 for temperatures of 298, 195, and 80 K. Individual points indicate the data, and the solid lines represent the least-squares fits. The statistical uncertainties (one standard deviation) for the broadening coefficients determined from the fits in Fig. 3 are 1–2%. Systematic errors, due to uncertainty in the dye-laser scan width, are about 1% or less.

Table I summarizes all of the N_2 self-broadening coefficients measured in this study. These values are graphically illustrated in Fig. 4 as a function of rotational quantum number. Odd- J transitions in N_2 were not studied. For $S(4)$ through $S(12)$, the specified uncertainties are one standard deviation for the least-squares fit. For $S(0)$, $S(2)$, $S(14)$, and $S(16)$, data were obtained at only one density, and the uncertainties shown for these transitions represent the error in the linewidth determination of a single-line profile.

Earlier room-temperature measurements by different authors^{3,6,7} have shown considerable disagreement (30%). Table II compares these earlier results with our present results. It can be seen that the three earlier studies show significant differences, while our current measurement is consistent with that of Ref. 7. The results of the three previous studies that are shown in Table II were obtained at densities where adjacent lines appreciably overlapped with one another, whereas the present results were obtained at densities where there was no overlapping. We postulate that the differences in the experimental results of the previous studies given in Table II are due to systematic errors arising from the overlapping of adjacent lines.

Theoretical calculations of the collision-broadened Raman linewidth have been performed by Grey and Van Kranendonk,¹¹ Srivastava and Zaidi,¹² and Robert and Bonamy.¹³ The difference in these three approaches is in the treatment of the short-range intermolecular interactions. The results of these different approaches are

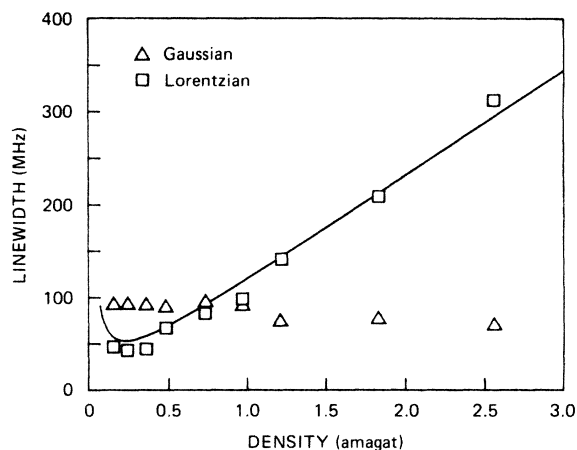


FIG. 6. Lorentzian (\square) and Gaussian (\triangle) components from Voigt fits to data as a function of density for $S(1)$ in H_2 . Solid line is a linear one-parameter fit to Eq. (1).

compared with our measurements in Fig. 5, where the room-temperature broadening coefficients are shown as a function of rotational quantum number J . We also show the experimental values of Jammu *et al.*³ for comparison. It should be noted that Srivastava and Zaidi¹² have used an adjustable parameter to obtain their fit to the data of Jammu *et al.*,³ whereas the calculations of Grey and Van Kranendonk¹¹ and Robert and Bonamy¹³ do not use any adjustable parameters. Figure 5 shows the *ab initio* calculations of Robert and Bonamy¹³ to be in the best agreement with our measurements.

To compare the pure rotational linewidths to the pure vibrational linewidths, we first note that the present rotational broadening coefficients are 10–15% larger than previously measured^{14–16} Q -branch vibrational broadening coefficients for low densities (0.1 amagat). Because negligible Doppler broadening of the rotational transitions means that Dicke narrowing is also negligible, the rotational line shapes are accurately described by Voigt profiles, while the vibrational transitions (with 20 times more Doppler broadening) require Galatry profiles for the most accurate fits. Also, because the vibrational transitions (0.3 cm^{-1}) are more closely spaced than the rotational (8 cm^{-1}) transitions, coherent line-mixing effects must be included to precisely describe the vibrational line shapes at densities of 1 amagat or larger.

Previous to this work, only atomic foreign-gas (He and Ar) broadening of the N_2 rotational transitions had been investigated.³ We have also measured diatomic foreign-gas (O_2) broadening coefficients at 195 and 295 K for the four strongest N_2 transitions. Our O_2 results in Table III

TABLE III. Temperature dependence of the foreign-gas (O_2) broadening coefficients of N_2 rotational Raman lines.

$S(J)$	B (MHz/amagat)	
	295 K	195 K
6	2970 ± 130	2690 ± 120
8	2770 ± 80	2600 ± 100
10	2750 ± 50	2410 ± 100
12	2450 ± 70	1980 ± 100

TABLE IV. H₂ rotational Raman parameters for an ortho:para ratio of 3:1.

T (K)	$S(J)$	ν_R (cm ⁻¹)	$\Delta\nu_D$ (MHz)	D_0^a (cm ² amagat sec ⁻¹)	A (MHz amagat)	ρ_c (amagat)
80	0	354	48	0.871	1.37	0.095
	1	587	80	0.493	2.10	0.088
295	0	354	92	1.19	1.87	0.068
	1	587	153	1.42	6.15	0.134

^aReference 18.

show that the foreign-gas broadening by O₂ is typically 85–90 % of the self-broadening at both temperatures. Thus the foreign-gas broadening by O₂ is approximately 30% larger than the foreign-gas broadening by the atomic gases.³

B. Line broadening in H₂

The Raman linewidth for H₂ has a much more complex density dependence than that for N₂. This results mainly from the fact that the H₂ density-broadening coefficient is approximately a factor of 30 smaller than the N₂ broadening coefficient, and thus Dicke¹⁷ or collisional narrowing of the Raman linewidth can be observed^{18,19} in the low-density regime if the resolution is high enough. A summary of the relevant collisional processes that contribute to the linewidth at various densities is given in Ref. 18.

For densities above a certain cutoff density (ρ_c defined below), the Raman line-shape function is Lorentzian with a FWHM linewidth $\Delta\nu$ that can be expressed as

$$\Delta\nu = A/\rho + B\rho, \quad (1)$$

where A (MHz amagat) is a coefficient proportional to the self-diffusion coefficient D_0 (cm² amagat sec⁻¹). For forward scattering,¹⁸ A is equal to

$$A = 4\pi^2\nu_R^2 D_0 \quad (2)$$

where ν_R is the Raman transition frequency in cm⁻¹.

This model is known as the diffusion model of the Raman linewidth and it diverges as the density approaches zero. There is a cutoff density, ρ_c , at which this model predicts a linewidth that is 10% larger than that predicted by the “hard collision” line-shape theory.¹⁸ We have previously determined that

$$\rho_c = 3.33A/\Delta\nu_D, \quad (3)$$

where $\Delta\nu_D$ (MHz) is the FWHM Doppler width of the Raman transition given by (forward scattering)

$$\Delta\nu_D = 7.15 \times 10^{-7} \nu_R (T/m)^{1/2}, \quad (4)$$

where ν_R is in MHz, T is the temperature in K, and m is the mass in amu. For densities larger than ρ_c , the line shape is Lorentzian and the widths can be effectively modeled using Eq. (1).

For example, the experimental data set for the $S(1)$ transition at 298 K is given in Fig. 6. From the Voigt fit, we determine both the Lorentzian and Gaussian contributions to the experimental linewidth. Since the Raman line shape is Lorentzian for all densities shown in Fig. 6, the Gaussian contribution is due to the spectral width of the pulsed dye laser. The Lorentzian and Gaussian contributions to the linewidth are plotted in Fig. 6, where we see that the Gaussian contribution is approximately constant while the Lorentzian contribution varies approximately linear in density.

Unfortunately, the 100-MHz resolution of our current laser system does not allow the Dicke narrowing of the H₂ rotational Raman linewidth to be resolved with any precision. We have therefore chosen a fitting procedure that uses D_0 determined from our previous study¹⁸ to calculate A from Eq. (2). The Lorentzian component of the experimental linewidth for densities larger than ρ_c is then fitted to Eq. (1) with one free parameter B . The parameters used in this fitting procedure are given in Table IV.

The density-broadening coefficients B determined using this procedure are given in Table V, where the uncertainties shown are one standard deviation for the one-parameter linear least-squares fit. This fit is illustrated by the solid line in Fig. 6 for the $S(1)$ transition. The maximum correction to the linewidth due to including the collisional narrowing term in Eq. (1) is on the order of 5–10 %.

We have also included in Table V data from the previous work of Van Den Hout *et al.*²⁰ and Cooper, May, and Gupta.²¹ There are small discrepancies with the results of Refs. 20 and 21. Some of these differences could be due to small errors in our estimate of A for these rotational transitions. We emphasize that the N₂ results of Sec. IIIA are free of this problem since Dicke narrowing is negligible.

TABLE V. Self-broadening coefficients for the rotational Raman lines of H₂.

$S(J)$	B (MHz/amagat)				
	This work	295 K		80 K	
		This work	Ref. 20	Ref. 21	This work
0	77±2	84±2	84±2	67±2	63±1
1	114±5	104±2	105±4	110±3	99±1

C. Line shifts in N₂ and H₂

In all of the above cases for which density-broadening measurements were reported, we have also made density line-shift measurements. In all cases the line shifts were only a few percent of the linewidth, and hence any asymmetries in the line shapes need to be carefully analyzed.

The asymmetry in Fig. 2 is typical of that observed in our data for the higher-density N₂ data. The lower-density N₂ data contained an asymmetry that occurred only further out in the wing of the spectral profiles. About 80% of the total number of line profiles at all densities and temperatures exhibited this small asymmetry, where the data were slightly larger than the symmetric fit on the high-frequency side of the line. Roughly 20% of the line profiles were symmetric and only rarely did the asymmetry appear such that the data were smaller than the fit on the high-frequency side. It was determined that this asymmetry was not due to the saturation of the detection system by either the probe beam or the Raman signal. By scanning the dye laser backwards, it was determined that the asymmetry always remains such that the data are larger than the fit on the high-frequency side of the line, where the high-frequency side corresponds to a larger Raman shift. For densities above 0.5 amagat and for the pump-laser intensities used here, this asymmetry is not consistent with the measured magnitudes of Stark effects in N₂.²² At this time we are unable to determine the cause of these asymmetries.

In N₂, both the self-density shifts and the O₂ foreign-gas density shifts were found to lie in the range 50–150 MHz/amagat for the transitions and temperatures discussed above. There was no uniform dependence with either temperature or quantum number *J*. More importantly, there were inconsistencies observed in both the data acquired during the course of a single day and in the data collected from day to day. These inconsistencies have forced us to conclude that the line-shift measurements in N₂ are substantially disturbed by the asymmetric line shapes. The data can, however, be used to establish an upper limit to the magnitude of the line shifts. For all transitions and temperatures indicated for N₂ in Tables I and III, the density line shifts are less than 150 MHz/amagat. Future elimination of the asymmetry would enable us to detect line shifts as small as 10 MHz/amagat with our current experimental apparatus.

The density shifts observed in H₂, unlike those in N₂, were free of the inconsistencies mentioned above. Data for *S*(1) in H₂ at 295 K are illustrated in Fig. 7, where the density shift is defined as

$$\delta v = \nu_R(\rho) - \nu_R(0), \quad (5)$$

where $\nu_R(\rho)$ is the Raman transition frequency at the density ρ . Hence a negative shift results in a smaller Raman frequency. Density shifts were plotted as a function of density difference between the sample and reference cells rather than density because data were collected for reference cell pressures of 50, 100, and 200 Torr. The temperature is 295 K for the data of Fig. 7. A summary of our H₂ density-shift results is given in Table VI, along with the results from Refs. 20 and 21. The agreement be-

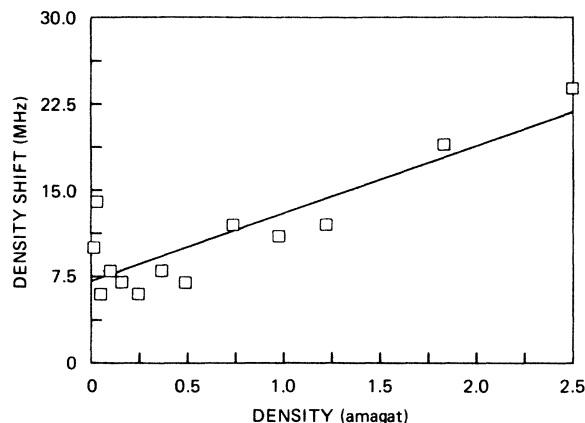


FIG. 7. Example of data for line-shift determination for *S*(1) in H₂ at 295 K. The solid line is the least-squares fit.

tween our results and those of Ref. 21 is consistent with the combined uncertainties for the two experiments.

It should be noted that the density shift for the rotational Raman line in H₂ is substantially different from that observed for the vibrational Raman lines.¹⁸ For example, at 80 K, the shift of the *Q*(1) vibrational transition is 13 times larger than the *S*(1) rotational Raman line. This difference results from the perturbation of the vibrational frequency of the H₂ molecule during an elastic collision, an effect not present for the rotational transition.

IV. DISCUSSION

A simple qualitative understanding of this temperature dependence for the N₂ rotational Raman broadening data given in Table I can be obtained from a consideration of Anderson's impact theory of the collisional broadening.²³ The linewidth can be expressed as

$$\Delta v = n \langle v \sigma(v) \rangle \simeq n \langle v \rangle \langle \sigma(v) \rangle, \quad (6)$$

where n is the molecular number density (cm⁻³), v is the relative velocity of the collision partners, σ is the collisional-broadening cross section, and the angular brackets denote an average over the velocity distribution of the gas. As can be seen from Eq. (6), the temperature dependence of the density-broadening coefficient is implicit in the velocity dependence of the collisional cross section. For example, if we assume a "hard-sphere" model for the cross section (velocity independent), the density-broadening coefficient ($\Delta v/n$) measured in our experiment would be proportional to $T^{0.5}$.

The broadening cross section is composed of contributions from several different types of collisions. Both elastic phase-perturbing collisions, and rotationally inelastic

TABLE VI. Temperature dependence of the density line shifts for H₂ rotational Raman lines.

<i>S</i> (<i>J</i>)	$\delta v = \nu_R(\rho) - \nu_R(0)$ (MHz/amagat)			
	295 K		80 K	
	This work	Ref. 21	This work	Ref. 20
0	6.5±3	3.1±1.5	-22.3±0.6	-22.3
1	5.9±1	4.0±1.5	-23.0±0.6	-17.8

collisions contribute to the linewidth. However, there are several cases where the contribution from elastic collisions is small. For example, the linewidth for isotropic vibrational Q -branch Raman scattering have no contribution from elastic collisions²⁴ if collisions perturb the ground and final vibrational level the same amount. This appears to be a good approximation for all cases except for hydrogen.¹⁸

Rotational Raman linewidths, on the other hand, have contributions from phase-perturbing elastic collisions. This is the primary reason why rotational Raman transitions usually have larger linewidths than vibrational Raman transitions. However, for the case of N_2 , CO , and CO_2 , it has been calculated¹¹ that elastic collisions contribute no more than 15% of the cross section. The present N_2 rotational linewidth measurements are 15% larger than the previous N_2 vibrational measurements,¹⁴⁻¹⁶ in good agreement with the conclusion that elastic collisions account for 15% of the rotational linewidths. Therefore, in most cases, the primary problem is to calculate the velocity dependence of the cross section for rotationally inelastic collisions.

The calculation of the collisional cross section has been the subject of considerable research. A good review of the various approaches to this calculation for Raman transitions has been given by Srivastava and Zaidi.²⁵ One approach to this calculation is to expand the long-range part of the intermolecular potential in a multipole expansion,^{11,23,25} and then calculate the contribution to the cross section of each term in this expansion. Using this approach, Gray and Van Kranendonk¹¹ have shown that for molecules such as N_2 , CO , and CO_2 , the most important terms in this expansion for self-broadening are the quadrupole-quadrupole (QQ) potential and the dispersion potential.

It can be shown²³ in general that the velocity dependence of these contributions to the cross section scales as

$$\langle \sigma \rangle \propto \langle v^{-2/(n-1)} \rangle, \quad (7)$$

where n is the exponent of the radial dependence of the long-range part of the potential in the form $V(r) \sim r^{-n}$. For the QQ potential, $n=5$, while for the dispersion potential $n=6$. Substituting Eq. (7) into Eq. (6) and remembering that $v \propto T^{0.5}$, we find that the density-broadening coefficient should scale with temperature as

$$(\Delta\nu/n) \propto T^{(n-3)/2(n-1)}. \quad (8)$$

From this simple argument, we would expect our density-broadening coefficients to scale as $T^{0.25-0.3}$, depending on the relative contribution to the cross section of the QQ and dispersion forces.

To test this simple model of the temperature dependence, we have fitted our data in Table I to the equation

$$B = B_0(T/295)^\gamma, \quad (9)$$

where B_0 is the density-broadening coefficient at 295 K. The results are given in Table VII as a function of initial rotational state. We find that $0.26 < \gamma < 0.39$, in reasonable agreement with this simple picture. We believe that most of the scatter in γ as a function of J is due to the

TABLE VII. Fit parameters for temperature dependence of density self-broadening coefficients in N_2 .

$S(J)$	B_0 (MHz amagat ⁻¹)	γ	C_0 (MHz amagat ⁻¹ K ⁻¹)
2	4160	0.33±0.02	6.8±0.4
4	3580	0.28±0.01	5.1±0.7
6	3560	0.26±0.04	4.8±0.1
8	3270	0.33±0.004	5.4±0.7
10	3060	0.35±0.002	5.2±0.6
12	2870	0.39±0.03	5.4±0.1

fact that a much larger temperature range needs to be investigated to accurately determine this small temperature dependence.

However, the scaling given in Eq. (9) may not be valid over a wide temperature range. By theoretically examining temperature dependence of the rotational Raman linewidth over a wide range, Pack²⁶ proposes a quadratic temperature scaling law for density-broadening coefficients that can be written as

$$B = B_0 + C_0(T - 295) + D_0(T - 295)^2, \quad (10)$$

where B_0 is the broadening coefficient at 298 K [same as in Eq. (9)], and C_0 and D_0 are fitting coefficients. We have previously used this temperature scaling formula in modeling Raman linewidths in H_2 .¹⁸ The data from Table I have been fitted to Eq. (10) assuming $D_0=0$, and the results are also given in Table VII. We find that this expression is just as useful as Eq. (9) in modeling the dependence of the density-broadening coefficient over the limited temperature range investigated in our experiment. Both Eqs. (9) and (10) can be used to predict B to better than 3% over the range of 80–300 K. Recent studies show that the temperature dependence for vibrational N_2 line shape is accurately described by a modified exponential gap scaling law²⁷ or a polynomial inverse energy-gap law.²⁸ Thus, although Eqs. (9) and (10) are useful for predicting low-temperature rotational Raman linewidths for N_2 , additional data (more data points covering a larger temperature region) are necessary to unambiguously determine the temperature dependence.

There are few molecular systems for which the rotational Raman linewidths have been determined as a function of temperature, and no other studies in N_2 . However, there have been extensive studies of the temperature dependence of absorption linewidths in CO (Ref. 29) and CO_2 .³⁰ The absolute magnitude of the linewidths determined from absorption will be different from those determined from Raman scattering. This is due to the fact that different states are involved in the calculation of the collision cross section. However, the temperature dependence will be similar if the same terms in the multipole potential are responsible for the broadening. This is the case¹¹ for both CO and CO_2 where the most important terms in the potential are the same as for N_2 .

Most of the data for linewidths in the literature are given in terms of pressure-broadening coefficients. We can compare results by noting that γ in Eq. (9) is related to η by $\gamma = 1 - \eta$, where η is the exponent of the tempera-

ture for pressure-broadening coefficients. The η values for the N_2 rotational Raman linewidths of this study cover a similar range of values as observed for the N_2 vibrational Raman linewidths²⁸ and the absorption linewidths in CO (Ref. 29) and CO_2 .³⁰

The details of the exact theoretical temperature dependence of the rotational Raman linewidths requires an *ab initio* calculation of the velocity-dependent collisional cross section, and is beyond the scope of this study. However, the precision of the data presented here should allow a detailed comparison with linewidths calculated from the various theoretical approaches thus allowing new theoretical advances to be made.

V. CONCLUSIONS

The density self-broadening coefficients have been measured at temperatures of 80, 195, and 295 K for the even- J rotational Raman transitions in N_2 . The temperature dependence of these coefficients was found to fit both linear and T^γ models to within 3%, however, additional temperature-dependent data are necessary to accurately determine the temperature dependence of these rotational

linewidths. The room-temperature results of this work are in agreement (less than 5% differences for $J > 2$) with the most recent *ab initio* calculations. Foreign-gas broadening of these N_2 transitions, due to O_2 , was also measured and found to be 10–15% smaller than the self-broadening coefficients. We have also determined that the density self-shifts and O_2 foreign-gas shifts for these same N_2 lines are no larger than 150 MHz/amagat. In a previous paper,² we have used the above results in the modeling of the temperature dependence of the steady-state Raman gain coefficient in N_2 .

The rotational Raman density broadening and shifts in H_2 were measured at 80 and 295 K. Our results were in general agreement with previous experimental work. This agreement of our H_2 data with other independent measurements provides confidence in the new temperature-dependent N_2 results presented above.

ACKNOWLEDGMENT

This work was supported by the Defense Advanced Research Projects Agency under Contract No. N00014-84-C-0256 through the U.S. Office of Naval Research.

-
- ¹M. Henesian, C. Swift, and J. R. Murray, *Opt. Lett.* **10**, 565 (1985).
- ²G. C. Herring, Mark J. Dyer, and William K. Bischel, *Opt. Lett.* **11**, 348 (1986).
- ³K. S. Jammu, G. E. St. John, and H. L. Welsh, *Can. J. Phys.* **44**, 797 (1966).
- ⁴G. V. Milahailov, *Zh. Eksp. Teor. Fiz.* **36**, 1368 (1959) [*Sov. Phys.—JETP* **9**, 974 (1959)].
- ⁵Yu A. Lazarev, *Opt. Spectrosc.* **13**, 373 (1962).
- ⁶F. Pinter, *Opt. Spectrosc.* **17**, 428 (1964).
- ⁷H. G. M. Edwards, D. A. Long, and S. W. Webb, *Self- and Foreign-Gas Broadening of the Pure Rotational Raman Lines of Oxygen and Nitrogen*, Proceedings of the 9th International Conference on Raman Spectroscopy, 1984 (unpublished) p. 760.
- ⁸P. Esherick and A. Owyong, in *Advances in Infrared and Raman Spectroscopy*, edited by R. J. Clark and R. E. Hester (Heyden, London, 1983), Vol. 9.
- ⁹Joseph O. Herschfelder, Charles F. Cartiss, and R. Byron Bird, *Molecular Theory of Gases and Liquids* (Wiley, New York, 1954).
- ¹⁰Philip L. Varghese and Ronald K. Hanson, *Appl. Opt.* **23**, 2376 (1984).
- ¹¹C. G. Grey and J. Van Kranendonk, *Can. J. Phys.* **44**, 2411 (1966).
- ¹²R. P. Shrivastava and H. R. Zaidi, *Can. J. Phys.* **55**, 542 (1977).
- ¹³D. Robert and J. Bonamy, *J. Phys. (Paris)* **40**, 923 (1979).
- ¹⁴G. J. Rosasco, W. Lempert, W. S. Hurst, and A. Fien, *Chem. Phys. Lett.* **97**, 435 (1983).
- ¹⁵M. L. Koszykowski, L. A. Rahn, and R. E. Palmer, *J. Chem. Phys.* (to be published).
- ¹⁶G. Millot, B. Lavorel, R. Saint-Loup, and H. Berger, *J. Phys. (Paris)* **46**, 1925 (1985).
- ¹⁷R. H. Dicke, *Phys. Rev.* **89**, 472 (1953).
- ¹⁸William K. Bischel and Mark J. Dyer, *Phys. Rev. A* **33**, 3113 (1986).
- ¹⁹B. K. Gupta and A. D. May, *Can. J. Phys.* **50**, 1747 (1972).
- ²⁰K. D. Van Den Hout, P. W. Hermans, E. Mazur, and H. F. P. Knapp, *Physica (Utrecht)* **104A**, 509 (1980).
- ²¹V. G. Cooper, A. D. May, and B. K. Gupta, *Can. J. Phys.* **48**, 725 (1970).
- ²²R. L. Farrow, and L. A. Rahn, *Phys. Rev. Lett.* **48**, 395 (1982).
- ²³B. H. Townes, and A. L. Schawlow, *Microwave Spectroscopy* (Dover, New York, 1975), pp. 368 and 369.
- ²⁴R. P. Srivastava and H. R. Zaidi, in *Raman Spectroscopy of Gases and Liquids*, edited by A. Weber (Springer, Berlin, 1979).
- ²⁵R. P. Srivastava and H. R. Zaidi, in *Raman Spectroscopy of Gases and Liquids*, edited by A. Weber (Springer, Berlin, 1979), pp. 167–198.
- ²⁶Russell T. Pack, *J. Chem. Phys.* **70**, 3424 (1979).
- ²⁷L. A. Rahn and R. E. Palmer, *J. Opt. Soc. Am. B* (to be published).
- ²⁸B. Lavorel, G. Millot, R. Saint-Loup, C. Wenger, H. Berger, J. P. Sala, J. Bonamy, and D. Robert, *J. Phys. (Paris)* **47**, 417 (1986).
- ²⁹Jeffrey N-P. Sun and Peter R. Griffiths, *Appl. Opt.* **20**, 1691 (1981); Prasad Varanasi and Sunil Sarangi, *J. Quant. Spectrosc. Radiat. Transfer* **15**, 473 (1975).
- ³⁰W. G. Planet and G. L. Tetterer, *J. Quant. Spectrosc. Radiat. Transfer* **22**, 345 (1979); Lloyd D. Tubbs and Dudley Williams, *J. Opt. Soc. Am.* **62**, 284 (1972); R. Ely and T. K. McCubbin, Jr., *Appl. Opt.* **9**, 1230 (1970).